Braincase With Natural Endocast of a Juvenile Rhinocerotinae From the Late Middle Pleistocene Site of Melpignano (Apulia, Southern Italy)

Dawid A. Iurino[1]*, Jacopo Conti[1], Beniamino Mecozzi[1,2] and Raffaele Sardella[1,2]

[1] PaleoFactory, Laboratory, Department of Earth Sciences, Sapienza University of Rome, Rome, Italy, [2] Department of Earth Sciences, Sapienza University of Rome, Rome, Italy

Cranial remains of juvenile fossil rhinoceroses are rarely described in literature and very few is known about the ontogenetic development of their inner anatomy. In this study, we report the first CT based description of a juvenile braincase and its natural brain endocast of a late Middle Pleistocene Rhinocerotinae from Melpignano (Apulia, Italy). The specimen belongs to an individual about 12–18 months old, representing to date the youngest Pleistocene rhinoceros of Mediterranean Europe documented by neurocranial material. Through digital visualization methods the neurocranium has been restored and the anatomy of both the brain and the paranasal sinuses has been obtained and compared with those of juvenile and adult Pleistocene rhinoceroses. We evidence a different morphological development of the inner cranial anatomy in fossil and extant African species.

Keywords: perissodactyla, paleoneurology, computed tomography (CT), virtual paleontology, digital cranial endocasts, paranasal sinuses

INTRODUCTION

During the Middle-Late Pleistocene, rhinoceroses were among the largest terrestrial mammals in European ecosystems together with proboscideans and hippopotamuses. They were represented by several taxa with different anatomical and ecological features, adapted to multiple environments from tropical scrublands and grasslands (Guérin, 1980) to cold glacial tundra (Deng et al., 2011; Boeskorov, 2012; Schreve et al., 2013). The finding in 17th century at Klagenfurt (Austria) of a woolly rhino *Coelodonta antiquitatis* (Blumenbach, 1799) skull was interpreted as a dragon and a six-tone statue of this legendary animal became the symbol of the Austrian town (Witton, 2018). By the start of 1800, fossils rhinoceroses have been recovered in Eurasia, Africa and America (Stuart, 1991; Lacombat, 2006; Markova et al., 2013; Faith, 2014), their taxonomy and phylogeny has been studied by several authors (Prothero et al., 1986; Cerdeño, 1995; Tong and Moigne, 2000; Antoine, 2003; Antoine et al., 2003; Piras et al., 2010; Deng et al., 2011; Steiner and Ryder, 2011; Welker et al., 2017; Cappellini et al., 2019) and even direct evidence of human interactions with the Late Pleistocene woolly rhinoceroses have been documented by cut marks

and cave paintings (Bello et al., 2009; Boeskorov, 2012; Chen and Moigne, 2018). Although some exceptionally preserved specimens are known (Voorhies and Stover, 1978; Voorhies, 1985; Protopopov et al., 2015), the Pleistocene fossil record of the European rhinoceroses is less abundant compared to those of other megaherbivores, and especially juveniles are scarce and their skull remains are rarely described in literature (Prothero, 2005; Shpansky, 2014). Therefore, taxonomic and ontogenetic studies are mostly focused on teeth, being more frequently recorded and of high diagnostic value (Garutt, 1994; Shpansky and Billia, 2006; Álvarez-Lao and García, 2011; Böhmer et al., 2016). To date, the number of juvenile specimens documented by partial or complete skulls is very low and mostly represented by Miocene taxa (**Table 1**). The only CT based study on a fossil Rhinocerotinae has been performed on "Sasha," a mummified calf of *C. antiquitatis* from the Semyulyakh River in Abyi District of Yakutia Republic (Russia) (Protopopov et al., 2015). Surprisingly, also the skull anatomy of the extant species has been scarcely investigated and very few studies on this topic have been reported (Bordoloi and Kalita, 1996; Borthakur and Bordoloi, 1997), especially those with x-ray techniques (Hieronymus et al., 2006; Gerard et al., 2018). Probably due to technical difficulties in performing CT scans on bulk and large skulls with conventional medical equipment. Consequently, many developmental and morpho-functional aspects of the skull pneumatization and the brain morphology are still almost completely unknown in extinct and extant rhinoceroses (Garrod, 1878; Bhagwandin et al., 2017). The most comprehensive ontogenetic studies on fossil Rhinocerotinae, based on external craniodental features, were conducted on *Chilotherium wimani* with nine complete skulls from the Late Miocene of China (Deng, 2001b), on *Teleoceras major* represented by 27 skulls from the Miocene of Nebraska (Hagge, 2010) and probably the largest sample of 399 mandibular fragments and limb bones from a minimum of 42 individuals of *C. antiquitatis* was reported by Shpansky (2014) from two Late Pleistocene sites in the Tomsk Priob'e area (south-east Western Siberia). In Europe, isolated and fragmentary cranial remains of juvenile fossil Rhinocerotinae have been occasionally reported (van der Made, 2010; Diedrich, 2013; Pandolfi et al., 2017; Giaourtsakis et al., 2006, 2018).

In this scenario, the juvenile specimen from the late Middle Pleistocene area of Melpignano (Apulia, Italy), represented by a partial braincase (MPND1082) and its natural brain endocast (MPND1083), offers a rare opportunity to describe the internal and external neurocranial features of a Pleistocene rhinoceros in an early ontogenetic stage.

GEOLOGICAL AND PALEONTOLOGICAL FRAMEWORK

The fossiliferous area of Melpignano (Lecce, Italy 40°08′20″ N, 18°16′23″ E) (**Figure 1**) is located in a region where several quarries are open for the extraction of a Miocene calcarenite, known as Pietra Leccese. Since the Pliocene (Ciaranfi et al., 1983), the calcarenite was affected by an intense karst activity that formed an articulated fissured network (Selleri et al., 2003;

Selleri, 2007). In the Melpignano area, these sub-vertical or funnel-shaped cavities exposed by the quarry activities and locally called "ventarole" are generally 1 m wide and up to 10 m high, filled with reddish clay-sands ("terre rosse") overlaid in some cases by brownish sediment ("terre brune") (Di Stefano et al., 1992; Bologna et al., 1994; Pandolfi et al., 2017). According to these authors, the chaotic arrangement of the bones in the sedimentary matrix, with any particular taphonomic pattern suggests that the origin of the deposit derived by the transport activity of the surface runoff waters and does not allow to define any stratigraphic succession. Moreover, based on faunal correlation of Melpignano assemblage with those from other paleontological sites of the Apulian area, the deposit has been initially assigned to the early Late Pleistocene (De Giuli, 1983; Bologna et al., 1994; Bedetti et al., 2004; Iurino et al., 2013; Pandolfi et al., 2017), although, a recent revision of the stratigraphic and fossil data suggests an older age of the site, referable to the late Middle Pleistocene (Mecozzi et al., 2019). A number of studies have focused on the rich vertebrate fauna of Melpignano, consisting of generally well preserved fossils with some articulated bones, attributed to: *Homo neanderthalensis*, *Palaeoloxodon antiquus*, *Equus ferus*, *Equus hydruntinus*, *Stephanorhinus hemitoechus*, *Hippopothamus amphibius*, *Dama dama*, *Cervus elaphus*, *Capreolus capreolus*, *Bos primigenius*, *Bison priscus*, *Sus scrofa*, *Canis lupus*, *Cuon alpinus*, *Vulpes vulpes*, *Panthera pardus*, *Felis silvestris*, *Lynx lynx*, *Crocuta crocuta*, *Meles meles*, *Mustela putorius*, *Lepus europaeus*, *Oryctolagus cuniculus*, *Erinaceus europaeus*, *Terricola savii*, *Apodemus sylvaticus*, and *Eliomys quercinus* (Mirigliano, 1941; De Giuli, 1980, 1983; Bologna et al., 1994; Bologna and Petronio, 1994; Pandolfi and Petronio, 2011; Bedetti et al., 2004; Iurino et al., 2013, 2015a; Vinuesa et al., 2016). The lack of signs of fluitation or long carrying on the surface of the fossil bones, suggests that the "ventarole" cavities have been probably filled in a short time span, collecting isolated bones and carcasses from the surrounding areas (Bologna et al., 1994). Furthermore, it is not excluded that these karst sinkholes worked as natural traps for living animals.

RHINOCEROTINAE FROM MELPIGNANO AREA

Starting from the second half of the last century, hundreds of fossil vertebrates, including rhinoceroses, have been collected from the fossiliferous area of Melpignano. Compared to other mammalian taxa, the fossil rhinoceroses are poorly documented and mostly represented by fragmented postcranial elements. The sample consists of about 25 specimens reported to date, excluding the material described herein. Considering the paucity, its taxonomic attribution has been problematic and has fueled a long debate among specialists. Indeed, the fossil rhinoceroses from Melpignano have been initially classified as *Rhinoceros* (= *Dicerorhinus*) *merckii* by Mirigliano (1941) and successively substituted as *nomen conservandum* with *Stephanorhinus kirchbergensis* (Jäger, 1835–1839) by Fortelius et al. (1993). This attribution was confirmed also by
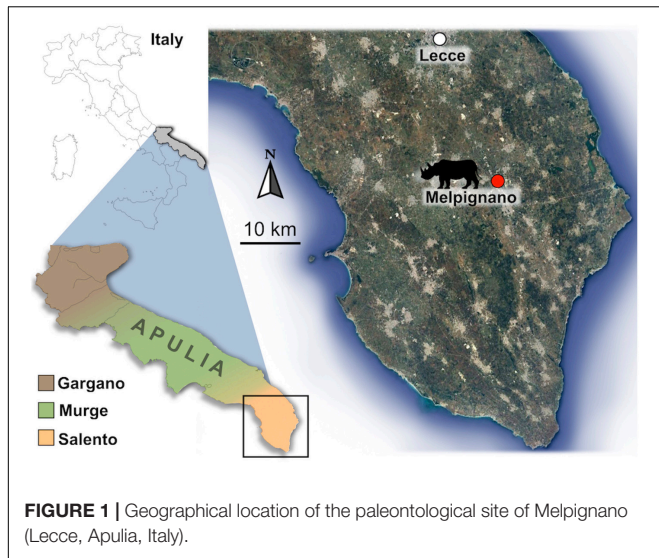
FIGURE 1 | Geographical location of the paleontological site of Melpignano (Lecce, Apulia, Italy).

Barbera et al. (2006). On the contrary, Petronio and Pandolfi (2008) attributed the material from Melpignano to a peculiar population of *Stephanorhinus hemitoechus* (Falconer, 1859), characterized by a reduced body-size compared to those reported from other European Middle Pleistocene sites. In the literature of the last decade, new fragmentary fossils have been reported from several Apulian sites as Avetrana, Grotta del Cavallo, Grotta del Sarcofago, Ingarano, Melpignano and Riparo l'Oscurusciuto, and all referred to *S. hemitoechus* (Pandolfi and Petronio, 2011; Pandolfi et al., 2017). Among the Apulian site, an exception is represented by the sample from Grotta Romanelli, which was attributed to three species: *Stephanorhinus hundsheimensis* and *Stephanorhinus* sp. from the level K and I respectively (Pandolfi et al., 2018); *Coelodonta antiquitatis* from the level I (Pandolfi and Tagliacozzo, 2013);

S. hemitoechus from the level G (Pandolfi et al., 2018). New unpublished material (limb bones) have been unearthed during the 2019 field activity at Grotta Romanelli and still under study.

MATERIALS AND METHODS

Studied Material

In early 1990s, the braincase and its natural brain endocast (**Figure 2**) were collected together within the reddish clay-sands from a small karst fissure in the Melpignano area during a field survey carried out by a research team of the Earth Sciences Department of Sapienza University of Rome, where the material is currently housed in the PaleoFactory laboratory. At the moment of discovery, the braincase was split in eight disarticulated elements partially covered by the sediment and positioned with the dorsal surface facing upwards, while the natural endocast has been detected within the brain cavity during the recovery process. In addition to the braincase, no other large mammalian bones have been found. The sample was labeled with progressive catalog numbers: MPND1082 (cranium) and MPND1083 (brain endocast).

For comparative purposes, we used the available literature of juvenile crania of fossil Rhinocerotinae (**Table 1**) and adult skulls of extant species.

For the material of the extant species, a CT scan of a head of a 41-years-old male *Ceratotherium simum* (Burchell, 1817) OUVC:9754 and an adult skull of *Diceros bicornis* (Linnaeus, 1758) have been downloaded from morphosource[1][2] and segmented with Mimics 20.0.

---

[1]http://www.morphosource.org/Detail/MediaDetail/Show/media_id/14624
[2]http://www.morphosource.org/Detail/MediaDetail/Show/media_id/39879

TABLE 1 | List of the fossil and extant specimens of juvenile Rhinocerotine considered from literature.

Taxon	Age	Locality	References
Dicerorhinus cixianensis	middle Miocene	Jiulongkou, Cixian (China)	Tong, 2012
Alicornps simorrense	middle Miocene	El Lugarejo or Arévalo (Spain)	Cerdeño and Sánchez, 2000
Acerorhinus yuanmouensis	Late Miocene	Yuanmou Basin (china)	Lu, 2013
Diceros gansuensis	Late Miocene	Housan, Linxia basin (china)	Deng and Qiu, 2007
Chilotherium wimani	Late Miocene	Laogaochuan, Fugu (china)	Deng, 2001a,b
Ceratotherium primaevum	Late Miocene	Oued el Hammam (Algeria)	Geraads, 2010
Paradiceros mukirii	Late Miocene	Fort Ternan (Kenya)	Hooijer, 1968; Geraads, 2010
Acerorhinus neleus	Late Miocene	Pikermi (Greece)	Giaourtsakis et al., 2018
Teleoceras major	Miocene	Ashfall Fossil Beds, Nebraska (USA)	Voorhies and Stover, 1978; Voorhies, 1985; Hagge, 2010
Stephanorhinus etruscus	late Pliocene	Blassac-La-Girondie (France)	Heintz et al., 1974
Coelodonta nihowanensis	Early Pleistocene	Shanshenmiaozui (China)	Tong and Wang, 2014
Stephanorhinus kirchbergensis	Late Pleistocene	Shennongjia (China)	Tong and Wu, 2010
Coelodonta antiquitatis	Late Pleistocene	Yakutia Republic of Siberia (Russia)	Protopopov et al., 2015

CT-Scanning

Tomographic images of the specimens were taken using a Philips Brilliance CT 64-channel scanner at M.G. Vannini Hospital (Rome). Both the natural brain endocast and the cranial elements were scanned entirely in the coronal slice plane from front to back. The scanning resulted in 355 slices for the braincase, 437 for the disarticulated braincase fragments and 263 for the brain endocast, with standard dimensions of 512×512 pixels. The slice thickness is 0.8 mm with an interslice space of 0.4 mm. CT image processing was performed using Mimics 20.0, while the digital restoration process and bone coloring were made with ZBrush 4R6.
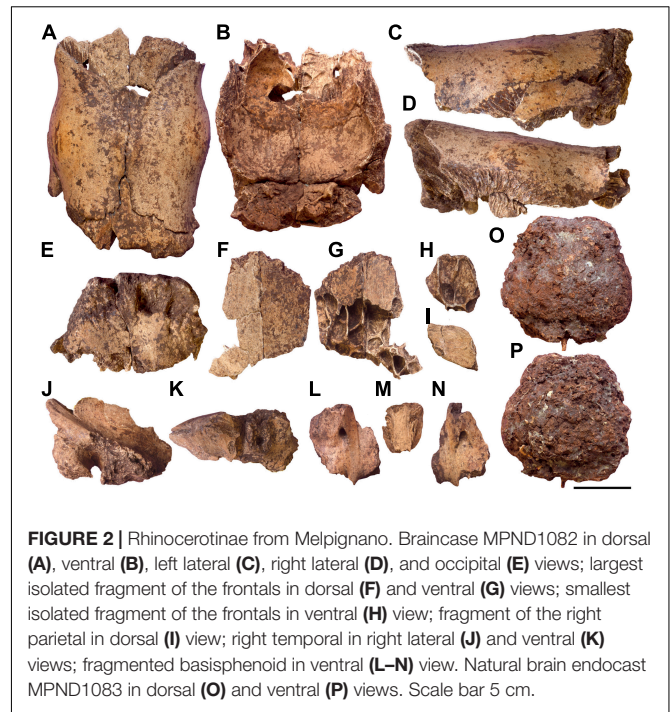
Virtual Restoration

Due to the fragility of the braincase, to avoid damaging the original material a digital restoration has been carried on. The virtual copies of all the fragments of the braincase have been manually reconnected matching the complementary margins of the bones (**Figures 3A–D**). The unavailability of skulls belonging to juvenile rhinoceroses prevented the digital acquisition of a 3D reference model for a restoration with geometric morphometric techniques. Despite this, the high correspondence of the fragments allowed obtaining a more complete version of the braincase. The basisphenoid (**Figures 3E–H**), obtained by the connection of three fragments is the only isolated bone due to the lack of connection edges with the restored braincase.

DESCRIPTION

Braincase
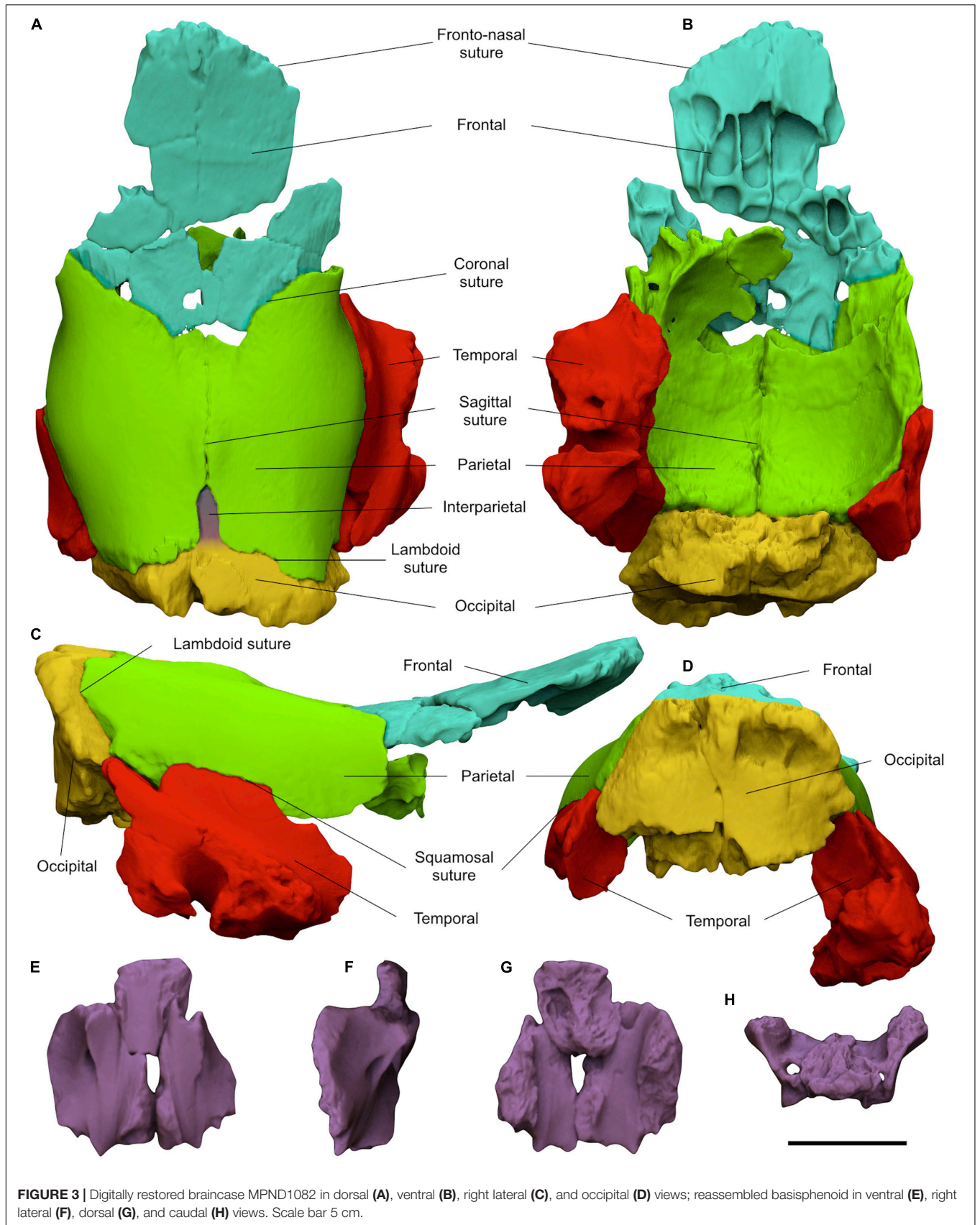
MPND1082 specimen (**Figures 2A–N** and **Supplementary Video S1**) is a partial juvenile braincase consisting of eight disarticulated elements in a good state of preservation. In dorsal view, the frontals are damaged and split in three portions, two isolated and one still articulated to the parietals. The dorsal surface of the largest isolated fragment is flat, and its anterior edge correspond to a quite damaged frontonasal suture. The parietals have a rounded and smooth surface, free of temporal lines and characterized by a butterfly-like outline (**Figure 2A**). Along the posterior margin of the parietals a marked notch receives a well-developed interparietal bone. The left side of the occipital is broken exposing the inner spongy bone tissue. The coronal, sagittal, and lambdoid sutures are clearly visible and unfused. In lateral view, the frontals are slightly projected upwards at the level of the coronal suture (**Figures 2C,D**). The parietals are dorsally quite flat with a small bulge crossed by the sagittal suture and located slightly in front of the interparietal bone. Anteriorly, the parietals are inflected forming a slight depression between the bulge and the coronal suture. On the left squamosal suture, a fragment of temporal is still connected to the parietal, whereas the right one is completely exposed and perfectly matches with the isolated fragment of the temporal. The caudal and basal portions of the right temporal are damaged, the zygomatic process is broken at the base, the external acoustic meatus is sub-elliptical in shape, the mastoid process is damaged, whereas the paraoccipital
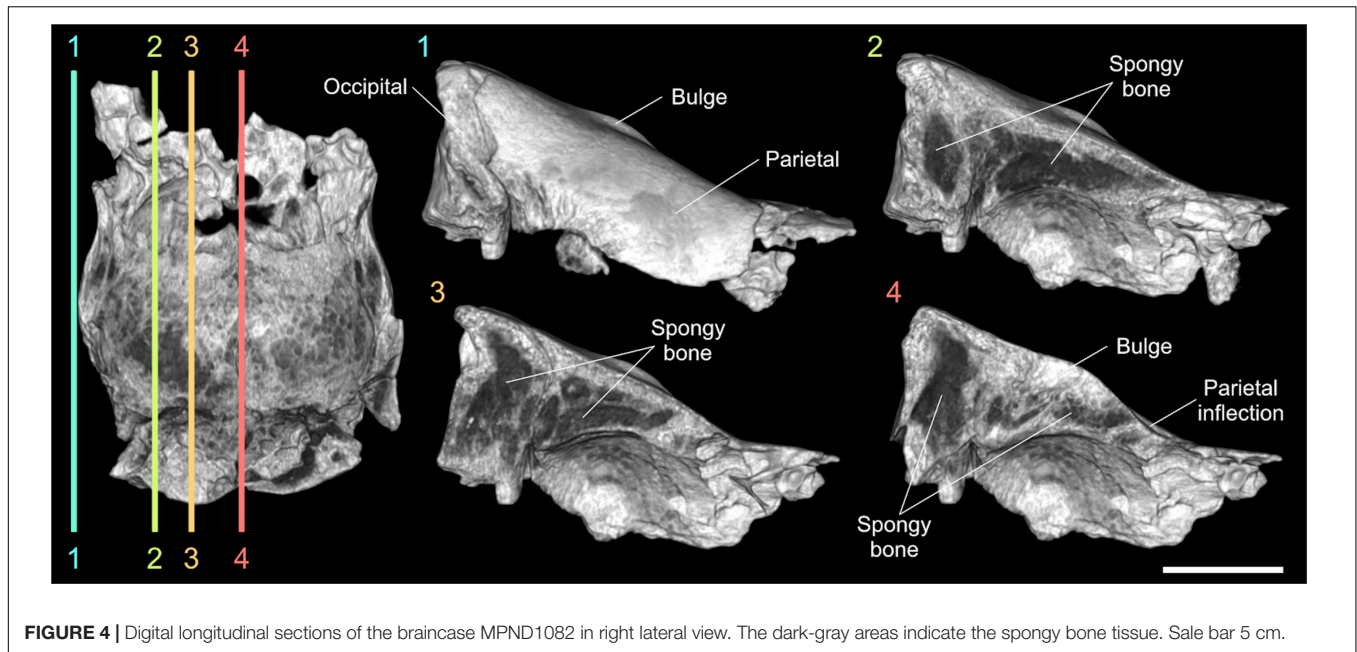

FIGURE 2 | Rhinocerotinae from Melpignano. Braincase MPND1082 in dorsal **(A)**, ventral **(B)**, left lateral **(C)**, right lateral **(D)**, and occipital **(E)** views; largest isolated fragment of the frontals in dorsal **(F)** and ventral **(G)** views; smallest isolated fragment of the frontals in ventral **(H)** view; fragment of the right parietal in dorsal **(I)** view; right temporal in right lateral **(J)** and ventral **(K)** views; fragmented basisphenoid in ventral **(L–N)** view. Natural brain endocast MPND1083 in dorsal **(O)** and ventral **(P)** views. Scale bar 5 cm.

and postglenoid processes are missing (**Figure 2J**). Dorsally, the occipital crest follows the flat profile of the parietals and is slightly projected backwards. In ventral view, the frontals show a series of asymmetrical small pneumatic cavities corresponding to the frontal sinuses (**Figure 2G**). The vault of the brain cavity is free of convolutions traces, except for some small grooves left by the blood vessels on the parietal lobes (**Figure 2B**). In caudal view, the preserved portion of the occipital shows a trapezoidal profile crossed by a deep fracture which cuts the bone in to two parts. The plane of the occipital surface is sub-vertical with a marked recess just below the occipital crest (**Figure 2E**). The basisphenoid is divided in three fragments and both caudal alar foramina are partially preserved (**Figures 2L–N**). Moreover, thanks to the virtual restoration, all the bone fragments have been reconnected and a slight curvature between the frontals and parietals at the level of the coronal suture has been evidenced (**Figure 3C**).

By processing CT images of all the cranial fragments we observed their inner structure, as the bone porosity and the fusion of the sutures, to estimate the age of the specimen. The longitudinal sections of the braincase evidenced a reduced bone density at the innermost portions of the occipital and the parietals, consisting of spongy bone tissue with no evidence of well-developed pneumatic chambers (**Figure 4**). A bone thickening is observed at the level of the parietal bulge along the sagittal plane. The spongy bone structure of the parietals is dorso-ventrally expanded close to the lambdoid suture and it thins noticeably under the parietal inflection just before the coronal suture (**Figure 4**). The reduced fusion of all the neurocranial sutures have been also highlighted through the CT images. The lambdoid suture shows wide empty spaces between the occipital and the parietals with smooth bone walls, whereas on the coronal

FIGURE 3 | Digitally restored braincase MPND1082 in dorsal **(A)**, ventral **(B)**, right lateral **(C)**, and occipital **(D)** views; reassembled basisphenoid in ventral **(E)**, right lateral **(F)**, dorsal **(G)**, and caudal **(H)** views. Scale bar 5 cm.

FIGURE 4 | Digital longitudinal sections of the braincase MPND1082 in right lateral view. The dark-gray areas indicate the spongy bone tissue. Sale bar 5 cm.

suture the bone tissue forms a hinge with very irregular and interdigitated bone margins. Concerning the paranasal sinuses, they are characteristic air-filled chambers developed in different cranial bones of placental mammals and are commonly divided into maxillary, frontal and sphenoidal sinuses (Falk, 2009; Boscaini et al., 2018). Processing the CT images of MPND1082, multiple chambers with a diameter just over 1 cm have been evidenced only in the frontal bones, thus corresponding to the frontal sinuses (**Figure 5C**). Such a pneumatization is missing inside the occipital, the parietals and the temporals, where instead, abundant spongy bone tissue is observed (**Figure 4**). In dorsal view, the frontal sinuses of MPND1082 are posteriorly delimited by the coronal suture with some terminal lobes that reach the anteriormost portion of the parietals, covering a large part of the frontal lobes of the brain (**Figure 5C**). Anteriorly, the air-filled chambers end 2 cm before the frontonasal suture in a completely different assessment compared to those of adult African rhinoceroses, where the frontal sinuses are part of a much extended and more complex system of cranial pneumatization (**Figures 5D–G**).
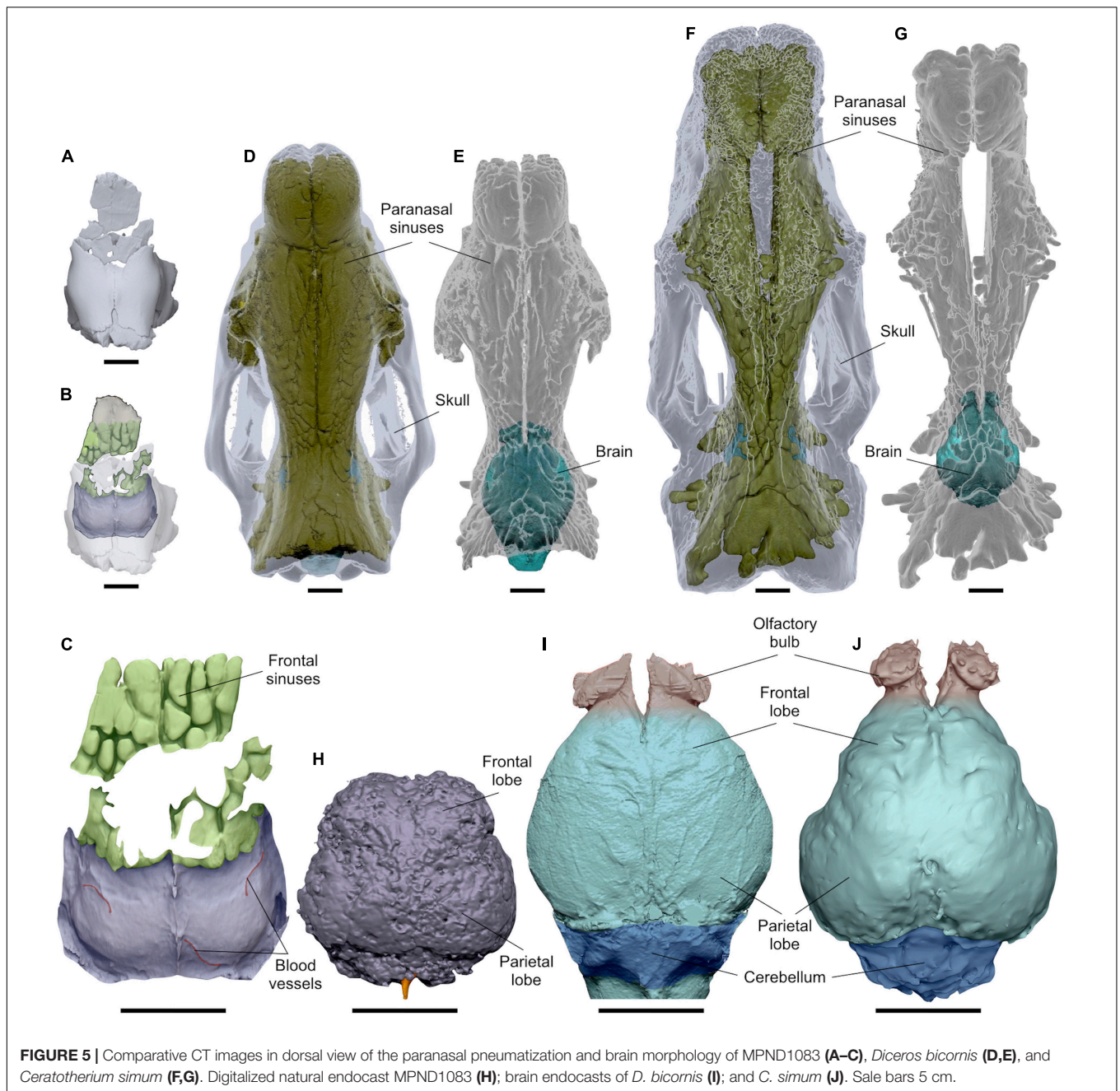
Natural Brain Endocast

A natural brain endocast is a brain replica obtained by the lithification of the sediment inside the brain cavity, a process that occurs only under specific sedimentary conditions (Hu et al., 2014; Ivanoff et al., 2014; Iurino et al., 2015b). The integrity of such a cast and the quality of its morphological details depend on multiple factors as the type and granulometry of the sediment, the amount of filling material and the presence of percolation waters depositing calcium. MPND1083 (**Figures 2O,P** and **Supplementary Video S2**) is a partial natural brain endocast mostly consisting of the telencephalon; olfactory bulbs are not preserved and the cerebellum seems almost completely missing. MPND1083 is globular in shape and is 97.3 mm long,

98.8 mm wide (maximum width) and 67.5 mm high with an approximate volume of 313 cm^3. The whole cast is formed by a poorly cemented sediment of fairly uniform granulometry and characterized by a reddish-brown color due to the iron oxides. Considering the fragility and the state of preservation of the specimen, only the general morphology of the telencephalon is appreciable. A gray-whitish patina partially enwraps some areas of the surface and corresponds to the residues of a consolidant agent applied in the early 1990s. In dorsal view (**Figure 2O**), the surface is irregular and affected by small cavities and fractures that prevent the identification of any morphological detail of the convolutions, blood vessels and nerves. Both cerebral hemispheres are preserved, but there is no evidence of the longitudinal fissure. The frontal lobes are less expanded than the parietal ones, which are divided from the cerebellum by a transverse fissure appreciable on the cast (**Figure 2O**). Unfortunately, the preserved portion of the cerebellum is too small and damaged to provide morphological and biometrical information. Along the broken portion of the cerebellum, a small coxal bone of a lagomorph partially protrudes from the sediment (**Figures 2O,P**). In ventral view, the brain cast is strongly damaged preventing any anatomical description (**Figure 2P**).

CT images (**Figure 6**) confirm the presence of several fracture lines of different thickness, ranging from 0.3 to 2.7 mm, which run irregularly within the natural endocast (**Figures 6E,F**). Some of these, especially the largest, are in continuity with the fractures visible on the surface with a pattern resembling those of the "mud cracks." A large number of empty sub-spherical holes ranging from 0.5 to 6.7 mm are arranged chaotically inside the specimen in partial overlap with the fractures (**Figures 6E,F**). Three small fragmented bones embedded and irregularly arranged in the sediment have been virtually extracted from the caudal portion of the endocast (**Figure 6G**). The size and morphology of these bones are compatible with those of a rabbit and consist of a left

FIGURE 5 | Comparative CT images in dorsal view of the paranasal pneumatization and brain morphology of MPND1083 **(A–C)**, *Diceros bicornis* **(D,E)**, and *Ceratotherium simum* **(F,G)**. Digitalized natural endocast MPND1083 **(H)**; brain endocasts of *D. bicornis* **(I)**; and *C. simum* **(J)**. Sale bars 5 cm.

calcaneus, a proximal epiphysis of a third right metatarsal and a right coxal bone, the latter partially exposed on the surface (**Figures 6H–J**).
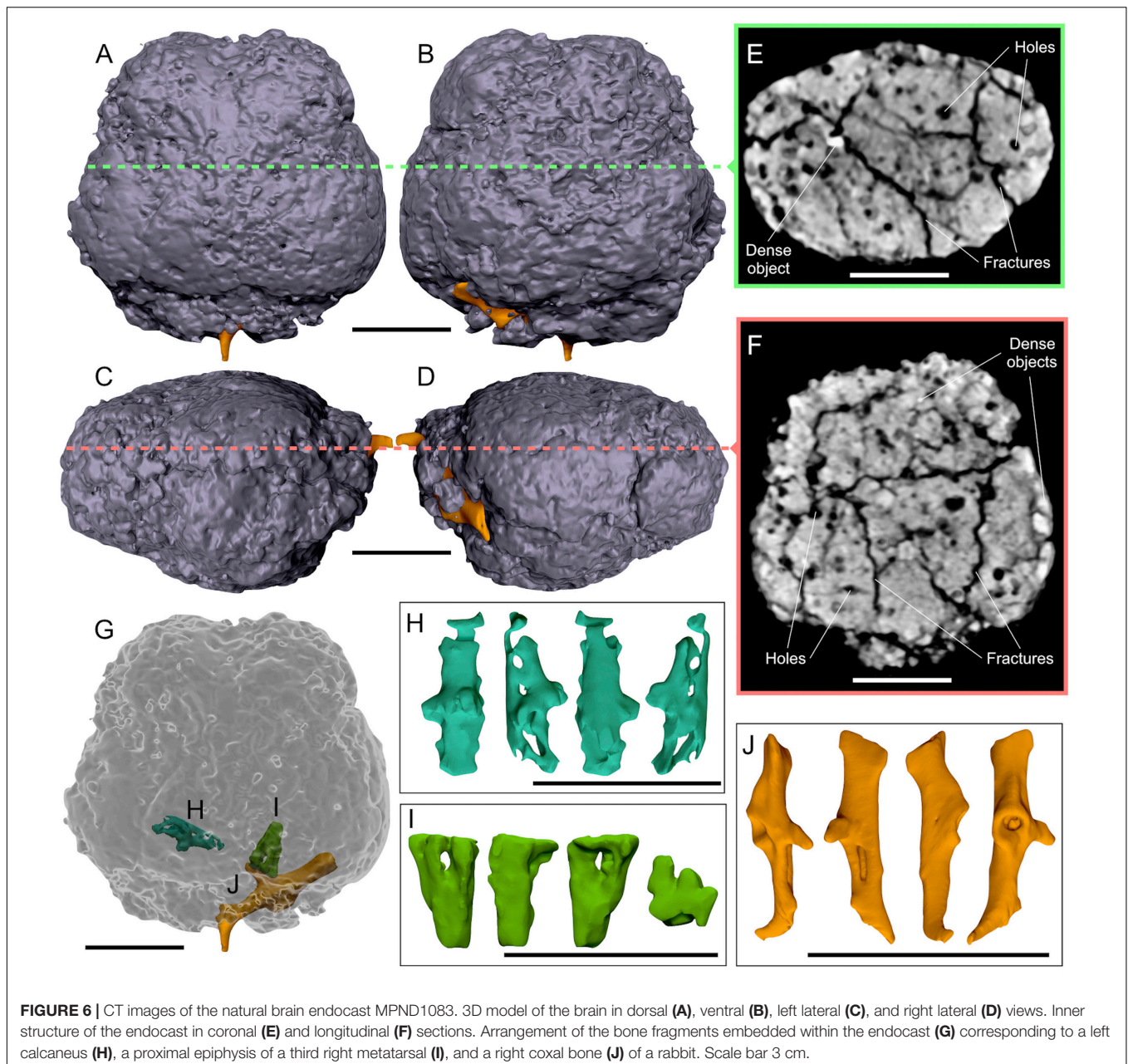
RESULTS

Virtual Endocasts

In addition to the digitalized natural endocast MPND1083, a second replica of the brain has been made using the braincase MPND1082 as a digital mold, which includes also a partial 3D model of the paranasal pneumatization (**Figures 5A–C**).

On this second endocast the size and the anatomical details of the surface are better appreciable. The cerebrum is globular, divided in two hemispheres by a longitudinal fissure both with smooth surface and free of convolutions (**Figure 5C**). Some tubular marks interpreted as blood vessels are noticeable along the parietal lobes close to the transverse fissure (**Figure 5C**). As the consequence of the weak fusion of the sagittal suture, the longitudinal fissure impressed on the digital cast would seem to be projected upwards, but this effect is a graphic artifact originated during the segmentation process. Indeed, the two main protrusions of the longitudinal fissure correspond with the slits observed along the sagittal suture (**Figure 5C**).

FIGURE 6 | CT images of the natural brain endocast MPND1083. 3D model of the brain in dorsal **(A)**, ventral **(B)**, left lateral **(C)**, and right lateral **(D)** views. Inner structure of the endocast in coronal **(E)** and longitudinal **(F)** sections. Arrangement of the bone fragments embedded within the endocast **(G)** corresponding to a left calcaneus **(H)**, a proximal epiphysis of a third right metatarsal **(I)**, and a right coxal bone **(J)** of a rabbit. Scale bar 3 cm.

Age Estimation

The unfused suture of the braincase and the volume of the natural endocast (313 cm^3), without the olfactory bulbs and cerebellum, of about half of those obtained for extant adult species (**Figures 5H–J**) indicate the early ontogenetic status of the fossil specimen. Considering the skull features, the development of the cranial sutures is similar in extinct and extant rhinoceroses species (Hagge, 2010). Therefore, we compared the Melpignano sample with extant and Miocene taxa, in order to better define the age of the individual (**Table 1**). The degree of fusion of the braincase sutures are compatible with those attributed to around 18-months-old specimen of *Coelodonta nihowanensis* (V 17616.1) from the early Pleistocene site of Shanshenmiaozui

(China) (Tong and Wang, 2014). The development of adult morphological characters, as the occipital crest pronouncement and temporal lines appearance, is similar among extinct and extant rhinoceroses, which appear during the age class III–V (2–4 years; Hagge, 2010). In extant rhinoceroses the lengthening of the cranium and the development of adult morphological characters start from the class age V to X (4–9 years), in which the cranium become wider and more angular in adult morphologies (Hagge, 2010). The lack of both temporal lines and the occipital crest pronouncement on the Melpignano braincase also contributes to indicate that the age of the individual was <2–4 years. An age of 4–5 months has been attributed to the cub of *C. antiquitatis* from the Late Pleistocene of Yakutia
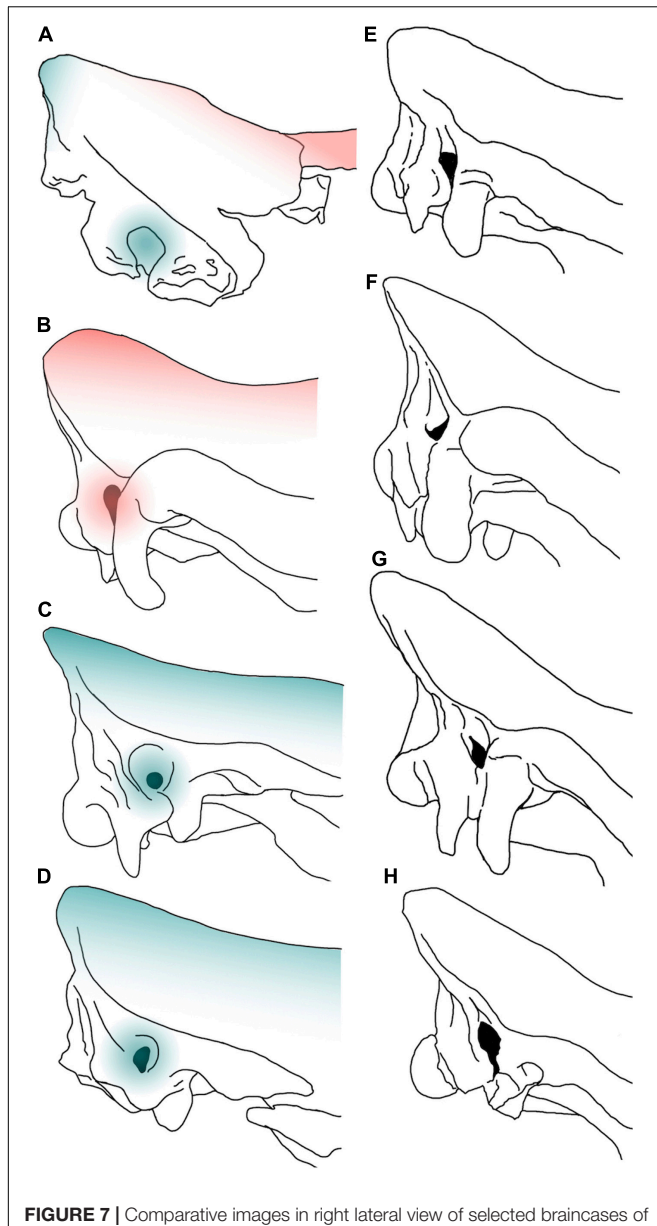
FIGURE 7 | Comparative images in right lateral view of selected braincases of juvenile **(A–D)** and adult **(E–H)** Pleistocene Rhinocerotinae from Eurasia. MPND1082 **(A)**, *Stephanorhinus kirchbergensis* No. H36 **(B)**, *Coelodonta antiquitatis* V 1453 **(C)**, *C. nihowanensis* V 17616.1 **(D)**, *S. etruscus* Mainz 1958/764 **(E)**, *S. kirchbergensis* from Spinadesco (Cremona, norther Italy) **(F)**, *S. hemitoechus* RGM 93302 **(G)**, and *C. antiquitatis* SfN **(H)**. The red-colored areas indicate the "*Stephanorhinus*" features, while the blue areas indicate the "*Coelodonta*" features evidenced on the juvenile specimens. The images are not to scale.

Republic (Russia) (Protopopov et al., 2015; Dirks et al., 2016), but unfortunately the exceptionally preserved fur partially cover the skull preventing the comparison. Finally, the juvenile cranium of the Late Pleistocene *Stephanorhinus kirchbergensis* (No. H36) from the Rhino Cave in Shennongjia (China), shows more fused sutures compared to the Melpignano braincase but the age was not estimated (Tong and Wu, 2010).

DISCUSSION

Age and Taxonomy

The specimen from Melpignano can be referred to a young individual, aged 12–18 months. In juvenile mammals, the process of bone development is intense and many of the diagnostic features used for taxonomic purposes, as well as for the sex determination, are not fully formed. The comparison with juvenile Pleistocene rhinoceroses (**Table 1** and **Figures 7A–D**) evidence how, in lateral view, the dorsal profile of MPND1082 shows a marked fronto-parietal angle compatible with that observed in *S. kirchbergensis* (No. H36) and noticeably different from *C. antiquitatis* (SJA 30, V 1453, "Sasha") and *C. nihowanensis* (IVPP V 17616.1), in which the fronto-parietal profile is almost flat. On the contrary, the lateral profile of the occipital crest is triangular with a narrow vertex in Melpignano and *Coelodonta* specimens, whereas it is more rounded and anteriorly projected in the juvenile *S. kirchbergensis* (**Figure 7B**). In caudal view, the latter (**Figure 7B**) shows a more marked dorso-ventral development of the occipital bone compared to MPND1082 and *Coelodonta* specimens (**Figures 7A,C,D**). The only comparative scheme of the auditory region in Rhinocerotinae was proposed by Loose (1975). The acoustic meatus of MPND1082 and wolly rhino specimens is quite broad and semicircular in shape, located in an advanced position with respect to the occipital plane. A different arrangement has been noticed in the juvenile and adult *S. kirchbergensis*, characterized by a drop-shaped meatus located in a more backward position close to the occipital plane (**Figures 7B,F**).

The combined set of *Coelodonta – Stephanorhinus* characters evidenced on the Melpignano specimen further complicates the taxonomic study and could be related to the young age of the individual. Being these two genera phylogenetically related (Piras et al., 2010; Deng et al., 2011; Welker et al., 2017; Cappellini et al., 2019) is likely that juveniles share similar morphological features.

Following the Hagge's (2010) scheme, the development of cranial features enables the identification of several age classes during the individual growth. Among these features, the occipital and temporal crests become more pronounced during the age classes X–XV (9–27 years) (Hagge, 2010).

This implies that the neurocranial portion in the juvenile rhinoceros offers a few information for taxonomy especially if compared with adult Pleistocene specimens (**Figures 7E–H**), being this region strongly involved during the ontogenetic development.

In the Melpignano area, fossil remains of adult *Stephanorhinus hemitoechus* have been reported by Petronio and Pandolfi (2008) and the young MPND1082 specimen could reasonably belong to this taxon. However, due to the lack of clear diagnostic features observable in the studied specimen, we refer the specimen to Rhinocerotinae to avoid circularity in the process of taxonomical attribution.

Nevertheless, the morphological differences detected in the auditory meatus rule out the attribution of MPND1082 to *S. kirchbergensis* and remarks the dubious presence of this taxon in southern Italy.
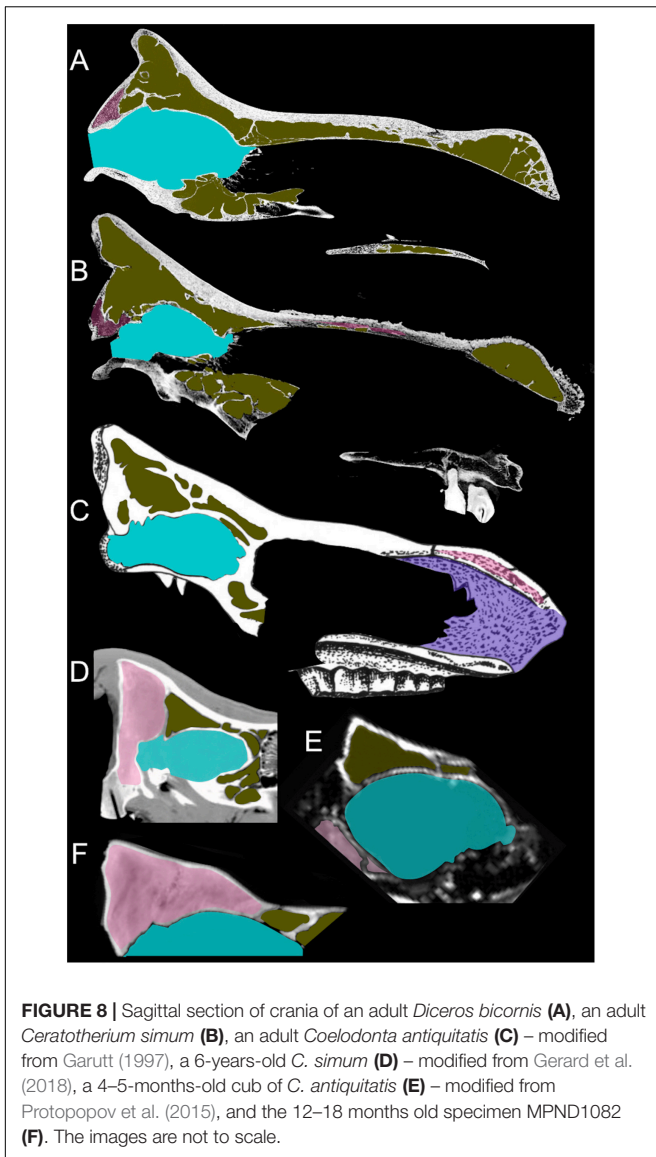
Brain

CT-scan devices have been largely used to obtain digital brain endocasts of a wide range of fossil vertebrates from different geological periods, including large mammals (e.g., Rowe et al., 2011; Knoll et al., 2012; Racicot and Colbert, 2013; Danilo et al., 2015; Forasiepi et al., 2016; Orihuela et al., 2019; Boscaini et al., 2018). Collecting and processing sensory information, the brain represents a fundamental organ for the interpretation of the sensory-perceptual ability in vertebrates, as well as its external morphology and volume can be addressed to anatomical and evolutionary studies (Dozo and Martínez, 2016; Vinuesa et al., 2016; Bertrand et al., 2017). Despite this, only few dated studies include paleoneurological aspects of fossil Rhinocerotinae (e.g., Gaudry and Boule, 1888), with the exception of the Late Pleistocene mummified cub of *C. antiquitatis* from the Yakutia Republic (Russia), whose CT images revealed the presence of several organs including brain tissue (Protopopov et al., 2015). Therefore, the MPND1083 represents one a few natural brain endocasts described in extinct Rhinocerotinae (**Figure 6**). MPND1083 consists of a globular telencephalon, free of convolutions with the frontal lobes less expanded than the parietal ones resembling in the general shape those reported on extant *Ceratotherium simum* and *Dicerorhinus sumatrensis* (Garrod, 1878; Bhagwandin et al., 2017), whereas it differs from that of *Diceros bicornis* (**Figure 5I**). In dorsal view, the brain of the black rhino shows a very rounded shape without the narrowing at the level of the lateral sulcus, which is evident in the other taxa. The different brain morphology of extant *D. bicornis* and *C. simum* (**Figures 5I,J**) has been studied with Magnetic Resonance Imaging by Bhagwandin et al. (2017) and related to diet. According to the authors, the shape of the brains reflects the overall architecture of the skulls, which in turn are related to the feeding habits of the two species, browsing for the black rhinoceros and grazing for the white rhinoceros. Such a relationship between brain morphology and feeding behavior in extant African rhinoceroses represent an interesting case study, which needs to be improved. Therefore, at the current status of knowledge we prefer to avoid any speculative morpho-functional inferences concerning the brain anatomy of the Melpignano specimen.

The lack of a detectable pattern of convolution observable on the Melpignano specimen as well as on both the adult African species (**Figures 5C,I,J**), seem not to be an age-related trait, since the brain endocasts of juvenile fossil mammals strongly resembles that of adults, indicating that the general brain morphology is almost completely formed in new-born individuals (Falk, 2009; Petrović et al., 2018). Among gyrencephalic mammals, large herbivores have less complex and very prominent convolutions compared to carnivorans (Roth and Dicke, 2005; Macrini et al., 2007; Hu et al., 2014), consequently, their brain endocasts have fairly smooth appearance amplified by the covering effect of the meninges. This condition is noticeable also on our sample of Rhinocerotinae brain endocasts.

The Paranasal Sinuses

Several hypotheses have been proposed to explain different patterns of cranial pneumatization documented in some mammalian taxa, which involve multiple ecological, morpho-functional and developmental factors (Farke, 2010). Such studies on rhinoceroses are almost completely missing (Gerard et al., 2018) and the development of cranial pneumatization in fossil and extant taxa was poorly investigated. The paranasal sinuses of adult *C. simum* and *D. bicornis* form a complex asymmetrical system of breached pneumatization in almost all the cranial bones, including the parietals and the occipital (**Figures 5D–G**). In contrast, in the MPND1083 specimen the pneumatization concerns only the frontal bones (**Figure 5C**) whereas the occipital and the parietals are filled by spongy-bone tissue without pneumatic cavities (**Figure 4**). It is likely that the areas filled with spongy bones could be developing in paranasal sinuses. In adult specimens of white and black rhinoceroses, the chambers are very wide and of irregular shape compared to those of the Melpignano cub, characterized by sub-spherical shape, arranged more regularly and with a diameter just over 1 cm. The longitudinal sections of the skull reveal different developmental patterns of the paranasal pneumatization across the considered sample (**Figure 8**). The adult skulls of extant African rhinoceros, *C. simum* and *D. bicornis* (**Figures 8A,B**), share a very wide pneumatization involving almost all the neurocranial bones, as well as the splanchnocranial region, which is interested by large nasal sinuses. The pneumatization of the occipital bone is completely developed in adults (**Figures 8A–C**) and still full of spongy bone tissue in the 6-years-old *C. simum* (**Figure 8D**; Gerard et al., 2018). In adult *C. antiquitatis* the lack of nasoconcal sinus and the strong reduction of the cranial pneumatization is considered a peculiar trait of this species (**Figure 8C**) as indicated also by other authors (Garutt, 1997; García-Fernández and Vicente, 2008; Shidlovskiy et al., 2012). In fact, the cranial architecture of adult woolly rhinoceros differs considerably from that of other fossil and extant rhinoceroses for a larger thickness of the nasal bones, a completely ossified nasal septum, a flat nasal horn and the retracted back of the occipital (**Figure 8C**). This strengthening of the cranial architecture and the expansion of the insertion areas of the neck muscles have been interpreted as an adaptation to sweep away large volumes of snow to reach the forage in Arctic environments (Boeskorov, 2012; Shidlovskiy et al., 2012). Curiously, the CT images of the abovementioned mummified cub of woolly rhino (Protopopov et al., 2015) show a wide empty chamber inside the cranium just up to the brain cavity, which involves the occipital, the parietal and the frontal bones (**Figure 8E**). A similar set of the cranial sinuses has been briefly documented by García-Fernández and Vicente (2008) on another Late Pleistocene *C. antiquitatis* from the Bown Bank site of the North Sea. It is not clear how much the contrast of the CT images reported by Protopopov et al. (2015) has affected the visibility of the spongy bone tissue, which, however, appears evident in some areas of the figure. In addition, the section of the skull at the level of the coronal suture confirms the presence of two large frontal sinuses, suggesting that in a

FIGURE 8 | Sagittal section of crania of an adult *Diceros bicornis* **(A)**, an adult *Ceratotherium simum* **(B)**, an adult *Coelodonta antiquitatis* **(C)** – modified from Garutt (1997), a 6-years-old *C. simum* **(D)** – modified from Gerard et al. (2018), a 4–5-months-old cub of *C. antiquitatis* **(E)** – modified from Protopopov et al. (2015), and the 12–18 months old specimen MPND1082 **(F)**. The images are not to scale.

4–5-months-old woolly rhino the cranial pneumatization was probably more developed than in the Melpignano braincase (**Figure 8F**), which is almost unpneumatized despite the older age of the individual. Wide neurocranial sinuses have been also documented in the 6-years-old white rhino mentioned above (Gerard et al., 2018), where the pneumatization is mostly represented by well-developed fronto-parietal sinuses with the occipital bone still completely filled by spongy tissue (**Figure 8D**). At the current state of knowledge, the reason of such an early and intense development of the skull pneumatization in juvenile woolly rhinoceroses and its paleoecological inferences are still unclear.

Taphonomy

The consistence of the Melpignano endocast is very friable and is crossed by several fracture lines, indicating a low degree of mineralization probably related to the low abundance of percolation water or its low mineral content. However, the overall size of the original specimen is comparable to the digital model obtained from the braincase MPND1082, with a reduction in thickness of about 5 mm in correspondence of the frontal and parietal lobes, indicating a weak erosive process that mainly affected the surface of the cast. Probably the presence of the braincase has performed a protective function against erosive agents, favoring the preservation of such a friable endocast.

CT analyses allowed to virtually extract three small bones embedded inside the natural cast (**Figures 6G–J**) represented by a left calcaneus, a third right metatarsal and a right coxal bone referred to *Oryctolagus cuniculus*. Both the heel and the metatarsal fragment, show a bad state of preservation. In particular, the external surface of the calcaneus is strongly altered and affected by several holes, whereas the inner portion is empty and the spongy bone tissue is missing. A similar deterioration could be due to weathering process or as a result of chemical aggression occurred during the digestion process of a medium-large predator (Horwitz, 1990).

The chaotic inner structure of the natural endocast and the presence of small mammal bones inside it, suggest a rapid burial and filling process of the skull with bone-rich sediments, whereas the lack of abrasions excludes a post-mortem transport of the braincase. The lack of signs of fluitation reported for other large fossil bones coming from the Melpignano area (Bologna et al., 1994) support the hypothesis that the karst sinkholes called "ventarole" probably worked more as natural traps rather than collectors of isolated bones and carcasses from the surrounding areas.

CONCLUSION

The study of juvenile specimens among mammals, relatively rare in the fossil record, is a promising topic, a source of information on the ontogeny and adaptations of extinct species. In particular, braincases and/or natural endocasts are of special interest and the use of CT scanning and digital analyses are a unique investigative tool. Nevertheless, the paucity of the available specimens of both extinct and extant taxa stresses as necessity of a larger set of information for this group, in order to better define the reconstruction of the ontogenetic development of different species of Rhinocerotidae and on their evolutionary framework.

However, for the juvenile Rhinocerothinae from the Middle Pleistocene of Melpignano tomographic images allowed to define the age of the individual and to analyze not only the hidden cranial anatomy, but also the inner structure of a natural endocast. The 3D models of the neurocranial cavities evidence the anatomical differences of the paranasal sinuses among the compared sample, including extinct and extant rhinoceroses. From the Melpignano area the occurrence of *Stephanorhinus hemithoechus* have been checked by different authors, but also other species have been described from other sites of the Italian Peninsula. The features of the Melpignano specimen cannot be considered fully diagnostic, therefore, to avoid circularity in the process of taxonomical attribution, we refer the specimen to Rhinocerotinae.

DATA AVAILABIITY STATEMENT

The datasets generated for this study are available on request to the corresponding author.

AUTHOR CONTRIBUTIONS

DI designed the research and wrote the manuscript with contribution of BM and RS. DI and JC processed and analyzed the CT images. All authors discussed the results and commented on the manuscript.

SUPPLEMENTARY MATERIAL

The Supplementary Material for this article can be found online at: https://www.frontiersin.org/articles/10.3389/feart. 2020.00094/full#supplementary-material

VIDEO S1 | 3D model of the braincase MPND1082.

VIDEO S2 | 3D model of the natural brain endocast MPND1083.

REFERENCES

Álvarez-Lao, D. J., and García, N. (2011). Southern dispersal and Palaeoecological implications of woolly rhinoceros (*Coelodonta antiquitatis*): review of the Iberian occurrences. *Quat. Sci. Rev.* 30, 2002–2017. doi: 10.1016/j.quascirev. 2011.05.005

Antoine, P. O. (2003). Middle Miocene elasmotheriine Rhinocerotidae from China and Mongolia: taxonomic revision and phylogenetic relationships. *Zool. Scr.* 32, 95–118. doi: 10.1046/j.1463-6409.2003.00106.x

Antoine, P. O., Duranthon, F., and Welcomme, J. L. (2003). *Alicornops* (Mammalia, Rhinocerotidae) dans le Miocčne supérieur des collines Bugti (Balouchistan, Pakistan): implications phylogénétiques. *Geodiversitas* 25, 575–603.

Barbera, C., Raia, P., and Meloro, C. (2006). I mammiferi di Melpignano conservati presso il Museo di Paleontologia di Napoli. *Thalassia Salentina* 29(Suppl. 2006), 237–243.

Bedetti, C., Pavia, M., and Sardella, R. (2004). Nuovi dati Sull'associazione a Vertebrati Fossili del Pleistocene Superiore di San Sidero, Maggio, (Puglia, SE Italia). IV Giornate di Paleontologia, Bolzano: Societá Paleontologica Italiana, 21–23.

Bello, S. M., Parfitt, S. A., and Stringer, C. (2009). Quantitative micromorphological analyses of cut marks produced by ancient and modern handaxes. *J. Archaeol. Sci.* 36, 1869–1880. doi: 10.1016/j.jas.2009.04.014

Bertrand, O. C., Amador-Mughal, F., and Silcox, M. T. (2017). Virtual endocast of the early Oligocene *Cedromus wilsoni* (Cedromurinae) and brain evolution in squirrels. *J. Anat.* 230, 128–151. doi: 10.1111/joa.12537

Bhagwandin, A., Haagensen, M., and Manger, P. R. (2017). The brain of the black (*Diceros bicornis*) and white (*Ceratotherium simum*) African rhinoceroses: morphology and volumetrics from magnetic resonance imaging. *Front. Neuroanat.* 11:74. doi: 10.3389/fnana.2017.00074

Blumenbach, J. F. (1799). *Handbuch der Naturgeschichte. Sechste Ausgabe*, 6th Edn. Göttingen: Johann Christian Dieterich.

Boeskorov, G. G. (2012). Some specific morphological and ecological features of the fossil woolly rhinoceros (*Coelodonta antiquitatis* Blumenbach, 1799). *Biol. Bull.* 39, 692–707. doi: 10.1134/s106235901208002x

Böhmer, C., Heissig, K., and Rössner, G. E. (2016). Dental eruption series and replacement pattern in Miocene *Prosantorhinus* (Rhinocerotidae) as revealed by macroscopy and X-ray: implications for ontogeny and mortality profile. *J. Mamm. Evol.* 23, 265–279. doi: 10.1007/s10914-015-9313-x

Bologna, P., Di Stefano, G., Manzi, G., Petronio, C., Sardella, R., and Squazzini, E. (1994). Late Pleistocene mammals from the Melpignano (LE) "Ventarole": preliminary analysis and correlations correlations. *Boll. Soc. Paleont. Ital.* 33, 265–274.

Bologna, P., and Petronio, C. (1994). The first occurrence of *Bison priscus* Bojanus in the Melpignano area (Lecce, southern Italy). *Boll. Soc. Paleont. Ital.* 33, 275–278.

Bordoloi, C. C., and Kalita, H. C. (1996). Gross anatomical studies of nasal cavity of rhino-calf (*Rhinoceros unicornis*). *Indian Vet. J.* 73, 470–472.

Borthakur, S., and Bordoloi, C. C. (1997). Gross anatomical study on the skull of adult rhino (*Rhinoceros unicornis*). *Indian Vet. J.* 74, 670–672.

Boscaini, A., Iurino, D. A., Sardella, R., Tirao, G., Gaudin, T. J., and Pujos, F. (2018). Digital Cranial Endocasts of the Extinct Sloth *Glossotherium robustum* (Xenarthra, Mylodontidae) from the Late Pleistocene of Argentina: Description and Comparison with the Extant Sloths. *J. Mamm. Evol.* 27, 55–71. doi: 10.1007/s10914-018-9441-1

Burchell, W. J. (1817). Note sur une nouvelle espèce de rhinocéros. *Bull. Soc. Philomath.* 1817, 96–97.

Cappellini, E., Welker, F., Pandolfi, L., Ramos-Madrigal, J., Samodova, D., Rüther, P. L., et al. (2019). Early Pleistocene enamel proteome from Dmanisi resolves *Stephanorhinus* phylogeny. *Nature* 574, 103–107. doi: 10.1038/s41586-019-1555-y

Cerdeño, E. (1995). Cladistic analysis of the family Rhinocerotidae (Perissodactyla). *Am. Mus. Novit.* 3143, 1–25.

Cerdeño, E., and Sánchez, B. (2000). Intraspecific variation and evolutionary trends of *Alicornops simorrense* (Rhinocerotidae) in Spain. *Zool. Scr.* 29, 275–305. doi: 10.1046/j.1463-6409.2000.00047.x

Chen, X., and Moigne, A. M. (2018). Rhinoceros (*Stephanorhinus hemitoechus*) exploitation in L evel F at the Caune de l'Arago (Tautavel, Pyrénéés-Orientales, France) during MIS 12. *Int. J. Osteoarchaeol.* 28, 669–680. doi: 10.1002/oa. 2682

Ciaranfi, N., Ghisetti, F., Guida, M., Iaccarino, G., Lambiase, S., Pieri, P., et al. (1983). Carta neotettonica dell'Italia meridionale. *Prog. Fin. Geod. Pub.* 515, 1–62.

Danilo, L., Remy, J., Vianey-Liaud, M., Mérigeaud, S., and Lihoreau, F. (2015). Intraspecific variation of endocranial structures in extant *Equus*: a prelude to endocranial studies in fossil equoids. *J. Mamm. Evol.* 22, 561–582. doi: 10.1007/s10914-015-9293-x

De Giuli, C. (1980). *La fauna di Maglie (Lecce). I Vertebrati Fossili Italiani, Catalogo della Mostra*. Verona: Museo civico di storia Naturale, 241.

De Giuli, C. (1983). *Le faune pleistoceniche del Salento. 1. La fauna di San Sidero 3.1 Quaderni*. Maglie, LE: Museo di Paleontologia di Maglie, 45–84.

Deng, T. (2001a). New materials of *Chilotherium wimani* (Perrisodactyle, Rhinocerotidae) from the Late Miocene of Fugu, Shaanxi. *Vert. Pal Asiat.* 39, 129–138.

Deng, T. (2001b). "Cranial ontogenesis of *Chilotherium wimani* (Perissodactyla, Rhinocerotidae)," in *Proceedings of the Annual Meeting of the Chinese Society of Vertebrate Paleontology*, Vol. 8, Beijing, 101–112.

Deng, T., and Qiu, Z. X. (2007). First discovery of *Diceros* (Perissodactyla, Rhinocerotidae) in China. *Vert. Pal Asiat.* 45, 287–306.

Deng, T., Wang, X., Fortelius, M., Li, Q., Wang, Y., Tseng, Z. J., et al. (2011). Out of Tibet: Pliocene woolly rhino suggests high-plateau origin of Ice Age Megaherbivores. *Science* 333, 1285–1288. doi: 10.1126/science.1206594

Di Stefano, G., Petronio, C., Sardella, R., Savelloni, V., and Squazzini, E. (1992). - Nuove segnalazioni di brecce ossifere nella costa fra Castro Marina e Otranto (Lecce). *Il Quat. Ital. Quat. Sci.* 5, 3–10.

Diedrich, C. (2013). Recycling of badger/fox burrows in Late Pleistocene loess by hyenas at the den site Bad Wildungen-Biedensteg (NW, Germany): woolly rhinoceros killers and scavengers in a mammoth steppe environment of Europe. *J. Geol. Res.* 2013:190795.

Dirks, W., Potapova, O., Witzel, C., Kierdorf, U., Kierdorf, H., and Protopopov, A. (2016). "Preliminary Report on the Deciduous Premolars of "Sasha", the First Infant Woolly Rhino (*Coelodonta antiquitatis*) to be discovered," in *Proceedings of the XIV Annual Meeting of the European Association of Vertebrate Palaeontologists*, Haarlem.

Dozo, M. T., and Martínez, G. (2016). First digital cranial endocasts of late Oligocene Notohippidae (Notoungulata): implications for endemic South American ungulates brain evolution. *J. Mamm. Evol.* 23, 1–16. doi: 10.1007/s10914-015-9298-5

Faith, J. T. (2014). Late Pleistocene and Holocene mammal extinctions on continental Africa. *Earth Sci. Rev.* 128, 105–121. doi: 10.1016/j.earscirev.2013.10.009

Falconer, H. (1859). Modifications apportés par Mr. Falconer a la faune du Val d'Arno. *Bull. Soc. Vaudoise Sci. Nat.* 6, 130–131.

Falk, D. (2009). The natural endocast of Taung (*Australopithecus africanus*): insights from the unpublished papers of Raymond Arthur Dart. *Am. J. Phys. Anthropol.* 140, 49–65. doi: 10.1002/ajpa.21184

Farke, A. A. (2010). Evolution and functional morphology of the frontal sinuses in Bovidae (Mammalia: Artiodactyla), and implications for the evolution of cranial pneumaticity. *Zool. J. Linn. Soc.* 159, 988–1014. doi: 10.1111/j.1096-3642.2009.00586.x

Forasiepi, A. M., MacPhee, R. D., Del Pino, S. H., Schmidt, G. I., Amson, E., and Grohé, C. (2016). *Exceptional Skull of Huayqueriana (Mammalia, Litopterna, Macraucheniidae) from the Late Miocene of Argentina: Anatomy, Systematics, and Paleobiological Implications*. New York, NY: American Museum of Natural History, 1–76.

Fortelius, M., Mazza, P., and Sala, B. (1993). *Stephanorhinus* (Mammalia: Rhinocerotidae) of the Western European Pleistocene, with a revision of *S. etruscus* (Falconer, 1868). *Palaeontogr. Ital.* 80, 63–155.

García-Fernández, D., and Vicente, J. (2008). Nuevas aportaciones al conocimiento de *Coelodonta antiquitatis* (Blumenbach, 1799) de Brown Bank, mar del Norte. *Butll. Cent d'Estud. Nat. Barc. Nord* 7, 309–329.

Garrod, A. H. (1878). On the Brain of the Sumatran Rhinoceros (*Ceratorhinus sumatrensis*). *Trans. Zool. Soc. Lond.* 10, 411–414. doi: 10.1111/j.1096-3642.1878.tb00467.x

Garutt, N. V. (1994). Dental ontogeny of the "woolly rhinoceros" *Coelodonta antiquitatis* (Blumenbach, 1799). *Cranium* 11, 37–48.

Garutt, N. V. (1997). Traumatic skull damages in the woolly rhinoceros, *Coelodonta antiquitatis* Blumenbach, 1799. *Cranium* 14, 37–46.

Gaudry, A., and Boule, M. (1888). *Matériaux Pour l'histoire des Temps Quaternaires*. Paris: Librairie F. Savy.

Geraads, D. (2010). "Rhinocerotidae," in *Cenozoic Mammals of Africa*, eds L. Werdelin and W. J. Sanders (Berkeley, CA: University of California Press), 675–689.

Gerard, M. P., Glyphis, Z. G., Crawford, C., Blikslager, A. T., and Marais, J. (2018). Identification of a nasoconchal paranasal sinus in the white rhinoceros (*Ceratotherium simum*). *J. Zoo Wildl. Med.* 49, 444–449. doi: 10.1638/2017-0185.1

Giaourtsakis, I., Svorligkou, G., and Roussiakis, S. (2018). "A juvenile skull of the hornless rhinocerotid *Acerorhinus neleus* (Rhinocerotidae, Mammalia) from the late Miocene locality of Pikermi (Attica, Greece)," in *Proceedings of the 62nd Annual Meeting Palaeontological Association*, ed. G. G. Lash (Bristol: University of Bristol).

Giaourtsakis, I., Theodorou, G., Roussiakis, S., Athanassiou, A., and Iliopoulos, G. (2006). Late Miocene horned rhinoceroses (Rhinocerotinae, Mammlia) from Kerassia (Euboea, Greece). *Neues Jahrb. Geol. Paläontol. Abh.* 239, 367–398.

Guérin, C. (1980). Les rhinoceros (Mammalia, Perissodactyla) du Miocene terminal au Pleistocene superieur en Europe occidentale: comparison avec les especes actuelles. *Doc. Lab. Géol. Fac. Sci. Lyon* 79, 1–1182.

Hagge, M. D. (2010). *A Functional and Ontogenetic Skull Analysis of the Extant Rhinoceroses and Teleoceras Major, an Extinct Miocene North American rhinoceros*. Ph.D. dissertation, Louisiana State University, Baton Rouge, LA.

Heintz, E., Guérin, C., Martin, R., and Prat, F. (1974). Principaux gisements villafranchiens de France: listes fauniques et biostratigraphie. *Mém. Bur. Recherches Géol. Minières* 78, 169–182.

Hieronymus, T. L., Witmer, L. M., and Ridgely, R. C. (2006). Structure of white rhinoceros (*Ceratotherium simum*) horn investigated by X-ray computed tomography and histology with implications for growth and external form. *J. Morphol.* 267, 1172–1176. doi: 10.1002/jmor.10465

Hooijer, D. A. (1968). A rhinoceros from the late Miocene of Fort Ternan, Kenya. *Zool. Meded.* 43, 77–92.

Horwitz, K. L. (1990). The origin of partially digested bones recovered from archaeological contexts in Israel. *Paléorient* 97–106. doi: 10.3406/paleo.1990.4522

Hu, Y., Chen, Y., Wang, S., and Sun, Q. (2014). Pleistocene equid brain endocast from Shanxi Province, China. *Acta Palaeontol. Pol.* 59, 253–259.

Iurino, D. A., Fico, R., Petrucci, M., and Sardella, R. (2013). A pathological Late Pleistocene canid from San Sidero (Italy): implications for social-and feeding-behaviour. *Naturwissenschaften* 100, 235–243. doi: 10.1007/s00114-013-1018-5

Iurino, D. A., Fico, R., and Sardella, R. (2015a). A pathological Late Pleistocene badger from San Sidero (Apulia, Southern Italy): implications for developmental pathology and feeding behaviour. *Quat. Int.* 366, 96–101. doi: 10.1007/s00114-013-1018-5

Iurino, D. A., Profico, A., Cherin, M., Veneziano, A., Costeur, L., and Sardella, R. (2015b). A lynx natural brain endocast from Ingarano (Southern Italy; Late Pleistocene): Taphonomic, Morphometric and Phylogenetic approaches. *Hystrix* 26, 110–117. doi: 10.4404/hystrix-26.2-11465

Ivanoff, D. V., Wolsan, M., and Marciszak, A. (2014). Brainy stuff of long-gone dogs: a reappraisal of the supposed Canis endocranial cast from the Pliocene of Poland. *Naturwissenschaften* 101, 645–651. doi: 10.1007/s00114-014-1200-4

Jäger, G. F. (1835–1839). *Über die Fossilen Säugetiere welche in Württemberg in Verschiedenen Formationen Aufgefunden Worden Sind, Nebst Geognotischen Bemerkungen Über Diese Formtionen*. Stuttgart: Erhard Verlag.

Knoll, F., Witmer, L. M., Ortega, F., Ridgely, R. C., and Schwarz-Wings, D. (2012). The braincase of the basal sauropod dinosaur *Spinophorosaurus* and 3D reconstructions of the cranial endocast and inner ear. *PLoS One* 7:e30060. doi: 10.1371/journal.pone.0030060

Lacombat, F. (2006). Morphological and biometrical differentiation of the teeth from Pleistocene species of *Stephanorhinus* (Mammalia, Perissodactyla, Rhinocerotidae) in Mediterranean Europe and the Massif Central, France. *Palaeontogr. Abt. A Band* 274, 71–111.

Linnaeus, C. (1758). *Systema Naturae per Regna tria Naturae, Secundum Classes, Ordines, Genera, Species, cum Characteribus, Differentiis, Synonymis, locis Editio decima, Reformata*. Laurentii: Salvii Holmiae.

Loose, H. (1975). Pleistocene Rhinocerotidae of W. Europe with Reference to the Recent Two-Horned Species of Africa and SE Asia. *Scr. Geol.* 33, 1–59.

Lu, X. (2013). A juvenile skull of *Acerorhinus yuanmouensis* (Mammalia: Rhinocerotidae) from the Late Miocene hominoid fauna of the Yuanmou Basin (Yunnan, China). *Geobios* 46, 539–548. doi: 10.1016/j.geobios.2013.10.001

Macrini, T. E., Rougier, G. W., and Rowe, T. (2007). Description of a cranial endocast from the fossil mammal *Vincelestes neuquenianus* (Theriiformes) and its relevance to the evolution of endocranial characters in therians. *Anat. Rec.* 290, 875–892. doi: 10.1002/ar.20551

Markova, A. K., Puzachenko, A. Y., Van Kolfschoten, T., Van der Plicht, J., and Ponomarev, D. V. (2013). New data on changes in the European distribution of the mammoth and the woolly rhinoceros during the second half of the Late Pleistocene and the early Holocene. *Quat. Int.* 292, 4–14. doi: 10.1016/j.quaint.2012.11.033

Mecozzi, B., Bellucci, L., Giustini, F., Iurino, D. A., Mazzini, I., and Sardella, R. (2019). "Large mammal fauna from the late Middle Pleistocene sites of Melpignano and San Sidero (Lecce, Southern Italy)," in *Proceedings of the XIX Edizione delle Giornate di Paleontologia Paleodays 2019* (New York, NY: Springer), 24.

Mirigliano, G. (1941). Avanzi di vertebrati quaternari di Melpignano (Lecce). *Atti Acad. Sci. Napoli.* 2, 1–46.

Orihuela, J., Viñola López, L. W., and Macrini, T. E. (2019). First cranial endocasts of early Miocene sirenians (Dugongidae) from the West Indies. *J. Vert. Paleontol.* 39:e1584565. doi: 10.1080/02724634.2019.1584565

Pandolfi, L., Boscato, P., Crezzini, J., Gatta, M., Moroni, A., Rolfo, M., et al. (2017). Late Pleistocene last occurrences of the narrow-nosed rhinoceros *Stephanorhinus hemitoechus* (Mammalia, Perissodactyla) in Italy. *Riv. Ital. Paleontol. Stratigr.* 123, 177–192.

Pandolfi, L., Fiore, I., Gaeta, M., Szabó, P., Vennemann, T., and Tagliacozzo, A. (2018). Rhinocerotidae (Mammalia, Perissodactyla) from the middle Pleistocene levels of Grotta Romanelli (Lecce, southern Italy). *Geobios* 51, 453–468. doi: 10.1016/j.geobios.2018.08.008

Pandolfi, L., and Petronio, C. (2011). The small-sized rhinoceroses from the Late Pleistocene of Apulia (Southern Italy). *Riv. Ital. Paleontol. Stratigr.* 117, 509–520.

Pandolfi, L., and Tagliacozzo, A. (2013). Earliest occurrence of the woolly rhino (*Coelodonta antiquitatis*) in Italy (Late Pleistocene, Grotta Romanelli site). *Riv. Ital. Paleontol. Strat.* 119, 125–129. doi: 10.1016/j.quaint.2011.06.051

Petronio, C., and Pandolfi, L. (2008). Stephanorhinus hemitoechus (Falconer, 1868) del Pleistocene superiore dell'area di Melpignano-Cursi e S. *Sidero* (Lecce, Italia). *Geol. Rom.* 41, 1–12.

Petrovič, V., Sabol, M., Šurka, J., Pyszko, M., and Stehlík, L. (2018). External brain morphology of juvenile cave hyena (*Crocuta crocuta spelaea*) from the Jasovská jaskyňa Cave (Slovakia) revealed by X-ray computed tomography. *Acta Geol. Slovaca* 10, 133–142.

Piras, P., Maiorino, L., Raia, P., Marcolini, F., Salvi, D., Vignoli, L., et al. (2010). Functional and phylogenetic constraints in Rhinocerotinae craniodental morphology. *Evol. Ecol. Res.* 12, 897–928.

Prothero, D. R. (2005). *The evolution of North American rhinoceroses*. Cambridge: Cambridge University Press.

Prothero, D. R., Manning, E., and Hanson, C. B. (1986). The phylogeny of the Rhinocerotoidea (Mammalia, Perissodactyla). *Zool. J. Linn. Soc.* 87, 341–366. doi: 10.1111/j.1096-3642.1986.tb01340.x

Protopopov, A., Potapova, O., Plotnikov, V., Maschenko, E., Boeskorov, G., Klimovskii, A., et al. (2015). "The frozen mummy of the woolly rhinoceros, *Coelodonta antiquitatis* (Blum., 1799) calf: a new data on early ontogenesis of the extinct species," in *Proceedings of the 75th Annual SVP Meeting*, Dallas, TX, 199.

Racicot, R. A., and Colbert, M. W. (2013). Morphology and variation in porpoise (Cetacea: Phocoenidae) cranial endocasts. *Anat. Rec.* 296, 979–992. doi: 10.1002/ar.22704

Roth, G., and Dicke, U. (2005). Evolution of the brain and intelligence. *Trends Cogn. Sci.* 9, 250–257.

Rowe, T. B., Macrini, T. E., and Luo, Z. X. (2011). Fossil evidence on origin of the mammalian brain. *Science* 332, 955–957. doi: 10.1126/science.1203117

Schreve, D., Howard, A., Currant, A., Brooks, S., Buteux, S., Coope, R., et al. (2013). A Middle Devensian woolly rhinoceros (*Coelodonta antiquitatis*) from Whitemoor Haye Quarry, Staffordshire (UK): palaeoenvironmental context and significance. *J. Quat. Sci.* 28, 118–130. doi: 10.1002/jqs.2594

Selleri, G. (2007). Karstic landscape evolution of southern Apulia fore- land during the Pleistocene. *Geogr. Fis. Dinamica Quat.* 30, 77–86.

Selleri, G., Sanso, P., and Walsh, N. (2003). The karst of Salento region (Apulia, southern Italy): constraints for management. *Acta Carsol.* 32, 19–28.

Shidlovskiy, F. K., Kirillova, I. V., and Wood, J. (2012). Horns of the woolly rhinoceros *Coelodonta antiquitatis* (Blumenbach, 1799) in the Ice Age Museum collection (Moscow, Russia). *Quat. Int.* 255, 125–129. doi: 10.1016/j.quaint.2011.06.051

Shpansky, A. V. (2014). Juvenile remains of the "woolly rhinoceros" *Coelodonta antiquitatis* (Blumenbach, 1799)(Mammalia, Rhinocerotidae) from the Tomsk Priob'e area (southeast Western Siberia). *Quat. Int.* 333, 86–99. doi: 10.1016/j.quaint.2014.01.047

Shpansky, A. V., and Billia, E. (2006). *Remains of Juvenile "Woolly Rhinos" Coelodonta antiquitatis Blumenbach, 1799) (Mammalia, Rhinocerotidae) from the Tomsk Ob' Region (Western Siberia)//Modern Paleontology: Classical and New Methods*. (Moscow: Russian Academy of Sciences), 103–108.

Steiner, C. C., and Ryder, O. A. (2011). Molecular phylogeny and evolution of the Perissodactyla. *Zool. J. Linn. Soc.* 163, 1289–1303. doi: 10.1111/j.1096-3642.2011.00752.x

Stuart, A. J. (1991). Mammalian extinctions in the Late Pleistocene of northern Eurasia and North America. *Biol. Rev.* 66, 453–562. doi: 10.1111/j.1469-185x.1991.tb01149.x

Tong, H., and Moigne, A. M. (2000). Quaternary rhinoceros of China. *Acta Anthropol. Sin.* 19(Suppl.), 257–263.

Tong, H., and Wu, X. (2010). *Stephanorhinus kirchbergensis* (Rhinocerotidae, Mammalia) from the Rhino Cave in Shennongjia, Hubei. *Chin. Sci. Bull.* 55, 1157–1168. doi: 10.1038/s41586-019-1555-y

Tong, H. W. (2012). Evolution of the non-*Coelodonta* dicerorhine lineage in China. *C. R. Palevol* 11, 555–562. doi: 10.1016/j.crpv.2012.06.002

Tong, H. W., and Wang, X. M. (2014). Juvenile skulls and other postcranial bones of *Coelodonta nihowanensis* from Shanshenmiaozui, Nihewan Basin, China. *J. Vert. Paleontol.* 34, 710–724. doi: 10.1080/02724634.2013.814661

van der Made, J. (2010). The rhinos from the Middle Pleistocene of Neumark-Nord (Saxony-Anhalt). *Veröff. Landesam. Denkmalpflege Archäol.* 62, 433–500.

Vinuesa, V., Iurino, D. A., Madurell-Malapeira, J., Liu, J., Fortuny, J., Sardella, R., et al. (2016). Inferences of social behavior in bone-cracking hyaenids (Carnivora, Hyaenidae) based on digital paleoneurological techniques: implications for human–carnivoran interactions in the Pleistocene. *Quat. Int.* 413, 7–14. doi: 10.1016/j.quaint.2015.10.037

Voorhies, M. R. (1985). A Miocene rhinoceros herd buried in volcanic ash. *Natl. Geogr. Soc. Res. Rep.* 19, 671–688.

Voorhies, M. R., and Stover, S. G. (1978). An articulated fossil skeleton of a pregnant rhinoceros, *Teleoceras major* Hatcher. *Proc. Nebr. Acad. Sci.* 88, 47–48.

Welker, F., Smith, G. M., Hutson, J. M., Kindler, L., Garcia-Moreno, A., Villaluenga, A., et al. (2017). Middle Pleistocene protein sequences from the rhinoceros genus *Stephanorhinus* and the phylogeny of extant and extinct Middle/Late Pleistocene Rhinocerotidae. *PeerJ* 5:e3033. doi: 10.7717/peerj.3033

Witton, M. P. (2018). *Palaeoartist's Handbook: Recreating Prehistoric Animals in Art*. Ramsbury: The Crowood Press.